

Direct Observation of Plugs and Intrawall Pores in SBA-15 Using Low Voltage High Resolution Scanning Electron Microscopy and the Influence of Solvent Properties on Plug-Formation

Tomas Kjellman,^{*,†} Shunsuke Asahina,[‡] Julien Schmitt,[§] Marianne Impérator-Clerc,[§] Osamu Terasaki,^{||,⊥} and Viveka Alfredsson[†]

[†]Physical Chemistry, Lund University, P.O. Box 124, SE-22100 Lund, Sweden

[‡]JEOL Ltd. SM BUSINESS UNIT, Akishima, Tokyo 196-8558, Japan

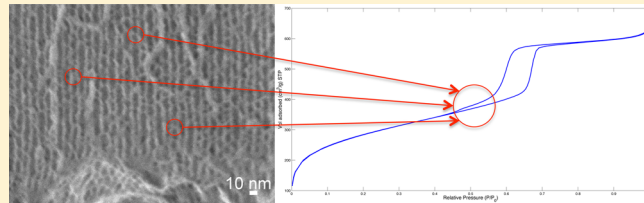
[§]Laboratoire de Physique des Solides, Université Paris Sud, UMR 8502, F-91405 Orsay, France

^{||}Graduate School EEWs WCU, Korea Advanced Institute of Science & Technology, 335 Gwahangno, Taejon 305701, Republic of Korea

[⊥]Department of Materials & Environmental Chemistry, Berzelii Center EXSELENT Porous Materials, Stockholm University, S-10691 Stockholm, Sweden

Supporting Information

ABSTRACT: Through the use of low voltage high resolution scanning electron microscopy (LV-HRSEM) we have studied the fine details of the intricate pore structure of SBA-15. Intrawall pores and deviations from the ideal and uniform cylindrical pores are clearly observed, and we report for the first time the direct observation of “plugs” in the pores. N₂-sorption measurements confirm their existence. LV-HRSEM provides an opportunity to quantify the frequency of occurrence of plugs within the pore structure. The rate of mesophase formation, followed with *in situ* small angle X-ray scattering (SAXS) under different solvent conditions, is shown to have a significant influence on the development of plugs and how frequently they occur. We suggest a mechanism explaining the existence of the plugs, providing means for a better understanding and control over material properties.



KEYWORDS: SBA-15, plugs, LV-HRSEM, intrawall pores, pore structure, *in situ* SAXS, N₂-sorption

INTRODUCTION

With the discovery of mesoporous silica materials^{1–3} a new field of materials research has evolved. Much effort is focused on developing materials for use in a wide range of applications.^{4–6} With each application comes a need for specific tailoring of the properties of the materials over several length scales, from subnanometer to micrometer and even to macroscopic properties.^{7,8} One of the most prominent mesoporous silica material, SBA-15, has a complicated porous structure. It consists of both uniform, 2D-hexagonally arranged, primary mesopores as well as unordered intrawall pores. This complementary set of intrawall pores is often referred to simply as microporosity, but this is a misnomer since they have a broad size distribution with a significant amount in the mesopore range. The intrawall pores have been shown to exist through the use of replication techniques, nitrogen and argon physisorption, and in some cases with high-resolution transmission electron microscopy.^{9–13} Another complicating aspect, namely, the existence of so-called “plugs” within the primary mesopores was shown by Van der Voort et al.^{14,15} and studied further by Kruk et al.¹⁶ using N₂- and Ar-sorption. A delayed desorption at the end of the expected H1 hysteresis shows how

the gas is hindered from escaping the primary mesopores. The presence of such obstructions/constrictions in the pores has been shown to lead to a significant loss of accessible pore volume upon grafting of a polymer to SBA-15 as the polymer seals off space only accessible to the probing gas molecules via the intrawall pores.^{17,18}

The use of scanning electron microscopy (SEM) for the analysis of porous materials has many benefits. In addition to supplying particle and morphology information, it affords surface information regarding mesopore openings and accessibility, providing that the resolution is sufficiently high. Because of electron-charging issues, conventional SEM requires conductive coating when investigating electric nonconductive materials. The use of a low accelerating voltage reduces charging of the sample but leads to an increase in size of the electron beam at the specimen surface and thus a decrease in resolving power. However, with the recent development of a low voltage high resolution scanning electron microscope (LV-

Received: August 4, 2013

Revised: September 18, 2013

Published: September 23, 2013

HRSEM) it is now possible to solve this issue and resolve fine details that are impossible to obtain with other techniques.^{19–21}

The synthesis of mesoporous silica with nonionic surfactants or polymers as structure directing agents is a straightforward procedure although a nontrivial system to understand. The interaction between silica and ethylene oxide (EO) has been established,^{22–24} and the assembly into an ordered structure is suggested to be driven mainly by hydrophobic interactions.²⁵ The lack of a sharp interface between the siliceous network and the organic micelles leads to the complicated pore system as described above. The inclusion of EO chains within the siliceous network has been explained as the cause of the above-mentioned intrawall pores^{12,13} and also to the pores suggested to exist in the plugs.^{14,15}

When additional species are introduced into a Pluronic containing synthesis solution it can affect the properties of the synthesized siliceous material.^{1,26} The effect can often be traced back to the influence of the added component on the solubility behavior of the Pluronic molecules,^{27,28} which has been studied intensely as a function of temperature,²⁹ the presence of salt,³⁰ and alcohols.³¹ The effect of salt is in accordance with the Hoffmeister series and includes both a general and a specific ion effect.³² The general ion effect leads to a decreased solubility because of increased polarity of the solvent, while the specific ion effect stems from the attraction of large, polarizable ions to the EO-part of the molecules, leading to an “effective” charging of the chains and hence an increased solubility.

When short-chain alcohols are added to an aqueous solution of Pluronic polymers it will favor demicellization because of an increased hydrophilicity (or rather solvophilicity) of the polymer.³¹ Thus it will induce the opposite effect on the Pluronic polymer as compared to the addition of a simple salt with salting-out properties.

In this paper we first describe the detection and analysis of the plugs in the primary mesopores, then discuss the dynamics of the formation events. This is followed by a discussion on the relation between the number of plugs and the solvent conditions leading up to the proposed mechanism for the formation of the plugs. Furthermore we show that LV-HRSEM clearly can detect intrawall pores in mesoporous materials synthesized with Pluronic polymers as structure promoter.

EXPERIMENTAL PROCEDURES

Synthesis of SBA-15. Pluronic P104 (12.5 g) was dissolved in 1.6 M HCl (483 g) to prepare a stock solution (2.5 wt %). A 18.75 g portion of the solution was placed in a Teflon lined polypropylene bottle alone or with addition of additives, either NaCl (0.55 or 1.10 g) or EtOH (0.43 or 0.86 g). The solution was then heated to 56 °C using a water bath with stirring (300 rpm). TMOS (0.68 mL) was added, and the stirring temporarily increased to 700 rpm for 1 min. After 24 h of synthesis the bottle was transferred to an oven for hydrothermal treatment at 80 °C under static conditions. This was followed by filtration, washing with H₂O and drying in atmosphere. Finally the dry material was calcined at 500 °C for 6 h. Samples with additives are denoted X_YM where X is the additive and Y is the final molar concentration of the additive in the solution. The reference material, synthesized without additives, is denoted SBA-15_ref.

A SBA-15 material synthesized using P123 as structure directing agent, and used in a previous study,³³ is used for comparison purposes and denoted SBA-15_P123.

LV-HRSEM. A high purity carbon stub was chosen for a sample support because of its high electric conductivity. The stub was first polished with a sandpaper (#1200) and then filter paper to make the surface sufficiently smooth to have good contact with the sample. Before mounting a sample, the stub was cleaned by ultra sonication in

ethanol followed by heating in a vacuum to remove alcohol. Calcined SBA-15 particles were picked on a swab (cotton ball) and dropped onto the stub and then heated in a vacuum oven for 10 min at 200 °C to dry before allowing to air-cool to room temperature. In addition, the samples were cleaned by Ar ion cleaner equipped in load lock chamber of LV-HRSEM instrument at 300 V for 10 min. The observed conditions including gun voltage, specimen bias, and so on are given for each LV-HRSEM image in figure captions. All images were taken with the in-column detector on a JEOL JSM-7800F GBSH.

In-Situ Small Angle X-ray Scattering (SAXS). Measurements were performed at the SWING beamline at SOLEIL (Energy 10 keV). The sample-CCD distance was 2 m, with a *q*-range: $5 \times 10^{-2} \leq q \leq 5.3 \text{ nm}^{-1}$. The *q*-range calibration was made using a silver behenate standard sample (*d*_{ref} = 58.38 Å). The measured intensity is always divided by the sample transmission.

For the absolute intensity calibration, scattering patterns of the empty capillary and the capillary filled with deionized water were always initially recorded. The value of the constant intensity contribution of water is equal to 0.016 cm⁻¹ on an absolute scale. Then, the signal of the same capillary filled with the solvent solution was recorded for subtraction purposes before the introduction of the synthesis solution. During each kinetics experiment, the capillary was kept fixed in the beam using a capillary holder, so that all patterns were recorded at the same position.

The reaction vessel was fitted with a closed loop of insulated Tygon tubing (length = 195 cm, volume of tubing = 3.92 mL) connected to a peristaltic pump, operating at a rate of approximately 20 mL/min through a 1.5 mL Quartz capillary with temperature control. A thermocouple was fitted in an unused capillary in the same sample holder to make sure the temperature in the capillary was kept at the same temperature as in the reaction vessel. To further minimize heat loss during the reaction, caused by the pumping, the synthesis solution was scaled up. The volume of P104-solution was 80 mL, and the other reagents were hence scaled up in accordance. The reactions were followed for between 30 and 40 min with one spectrum recorded every 30 s after the initiation time of 120–130 s.

SAXD. Measurements of the calcined material were performed on a GANESHA SAXS system (SAXSLAB, Denmark) with the used configuration yielding a *q*-range of 0.06–0.26 Å⁻¹. The powder samples were placed in quartz capillaries that were sealed with wax before being placed in the instrument. Unit-cells were determined from the position of the 10 peak.

N₂-Sorption. Nitrogen physisorption measurements at 77 K were performed on an ASAP 2400 instrument (Micromeritics Co., Norcross, GA). The Brunauer–Emmett–Teller (BET) method was used to deduce the surface area (*P/P*₀ = 0.05–0.02) and the total mesopore volume was taken at *P/P*₀ = 0.99. The mesopore size was determined by DFT analysis using the DataMaster software (Micromeritics Co., Norcross, GA).

RESULTS AND DISCUSSION

Analysis of Plugs in SBA-15. Several experimental techniques were used to characterize the synthesized materials, and the collected data is summarized in Table 1. LV-HRSEM images of materials NaCl_0.5M, SBA-15_ref and EtOH_0.5M, imaged perpendicular to the primary pores, are shown in Figure 1.

From direct observation it is clear that the pores are not ideal, straight cylinders as they tend to be described and depicted in the literature. Rather, they appear to be composed of smaller, quite corrugated, cylindrical segments of varying length, aligned along the same axis, separated by a thin silica wall, or plug (examples indicated by arrows in Figure 1). It should be noted that previous work by Tüysüz et al. includes HRSEM images of MCM-41 and SBA-15, and mentions constrictions in these materials.¹⁹ It is possible that these are indeed the plugs discussed in the present work. By marking subsequent cylindrical segments in black and plugs in white

Table 1. Material Properties of SBA-15, As Analyzed by N₂-Sorption, LV-HRSEM, in-Situ SAXS, and SAXD^{a,b}

sample name	BET (m ² /g)	V _t (cm ³ /g)	D (nm)	a ₀ (nm)	t _{Bragg} (min)	S _{Av} (nm)
EtOH_1M	938	0.85	7.85	10.2	—	26
EtOH_0.5M	1018	0.97	8.28	10.6	17	40
SBA-15_ref	1023	1.06	8.28	10.7	12	41
NaCl_0.5M	886	0.73	8.28	10.2	7.5	68
NaCl_1M	799	0.86	7.85	9.9	—	76

^aThe data are from calcined materials except the time for the appearance of the first Bragg peak (t_{Bragg}). ^bBET is the surface area, V_t the total pore volume, D the pore diameter, a₀ the unit cell parameter, t_{Bragg} the time of appearance of the first Bragg reflection, and S_{Av} the average distance between plugs.

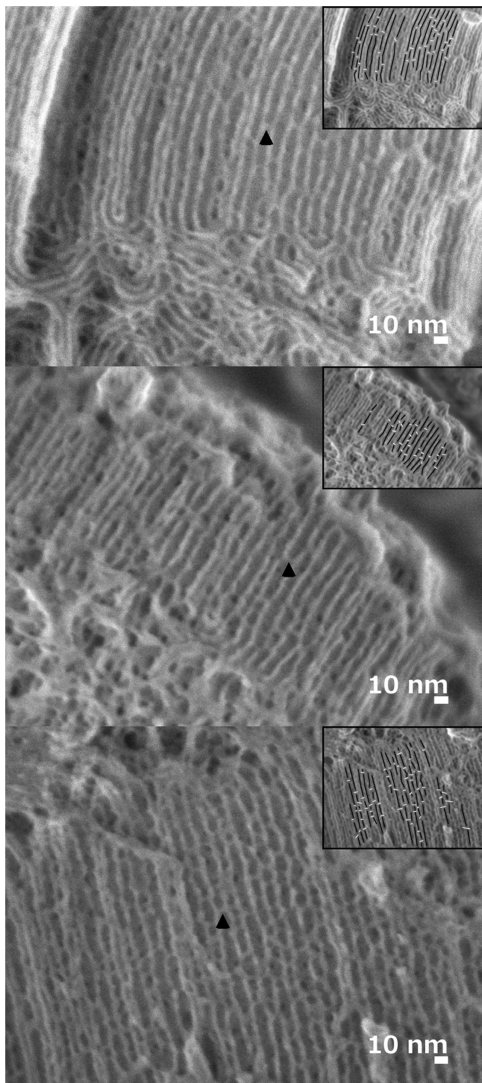


Figure 1. LV-HRSEM images of the calcined of samples NaCl_0.5 M (top), SBA-15_ref (middle) and EtOH_0.5 M (bottom). The black arrows show examples of plugs. The inset is showing the same image after analysis, with pores marked in black and plugs in white. Images were taken with a landing energy of 300 eV after applying a specimen bias of -5 kV.

(shown in insets of Figure 1 and Supporting Information, Figure S1) the number of plugs per unit length of pore can be analyzed. To take into account that the average particle

thickness is not the same for all materials, the ends of each measured pore are not considered as a plug. Under the conditions used for the LV-HRSEM observation of these materials, only the very top surface is resolved. The landing energy of the electrons of 300 eV gives a maximum penetration depth of roughly 5 nm (Supporting Information, Figure S2). The electrons that escape from the specimen to form the secondary electron image are estimated to come from approximately 20% of the maximum penetration depth (i.e., 1 nm). Hence it is not possible from this LV-HRSEM investigation to determine the level of constriction on the pore, that is, if the plug seals off the pore completely or only partially. While the plugs are clearly resolved with LV-HRSEM it is important to verify that they are not just present in the pores on the external surface of the particles but indeed present in the interior of the material as well. Therefore, the samples were investigated using N₂-sorption and the data obtained is included in Table 1. As can be seen in Figure 2, all samples

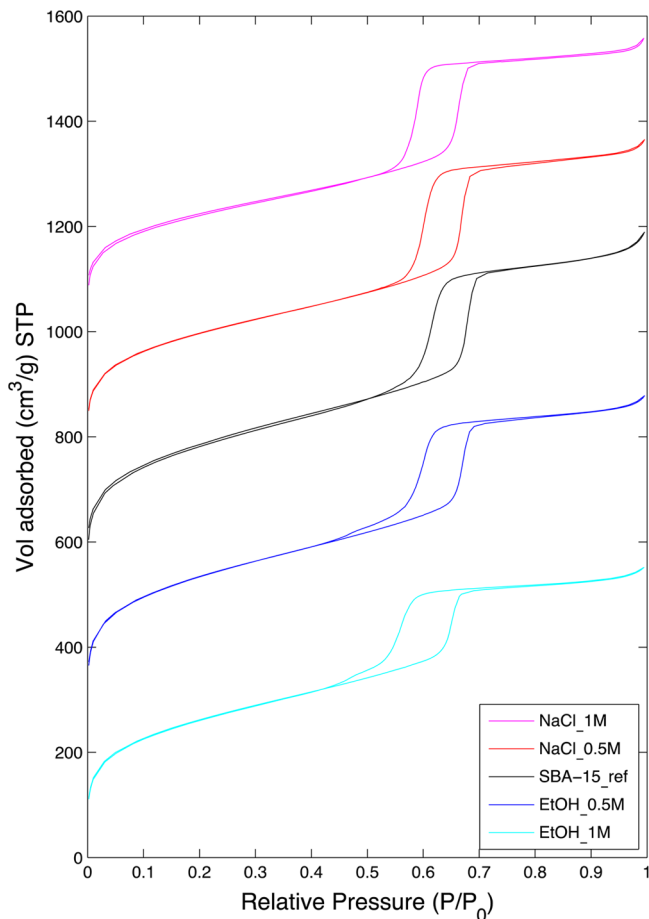


Figure 2. N₂-sorption isotherms of samples EtOH_1M, EtOH_0.5M, SBA-15_ref, NaCl_0.5 M, and NaCl_1M, offset for clarity by 0, 250, 500, 750, and 1000, respectively.

display the expected H1 hysteresis, but with a varying degree of tailing at the closing of the hysteresis, consistent with the presence of plugged pores^{14–16} and attributed to the pore blocking effect most commonly seen in so-called ink bottle pores.³⁴

This validates that plugs observed by LV-HRSEM are not simply a surface effect but indeed present throughout the porous structure. It is also clear from the isotherms (Figure 2)

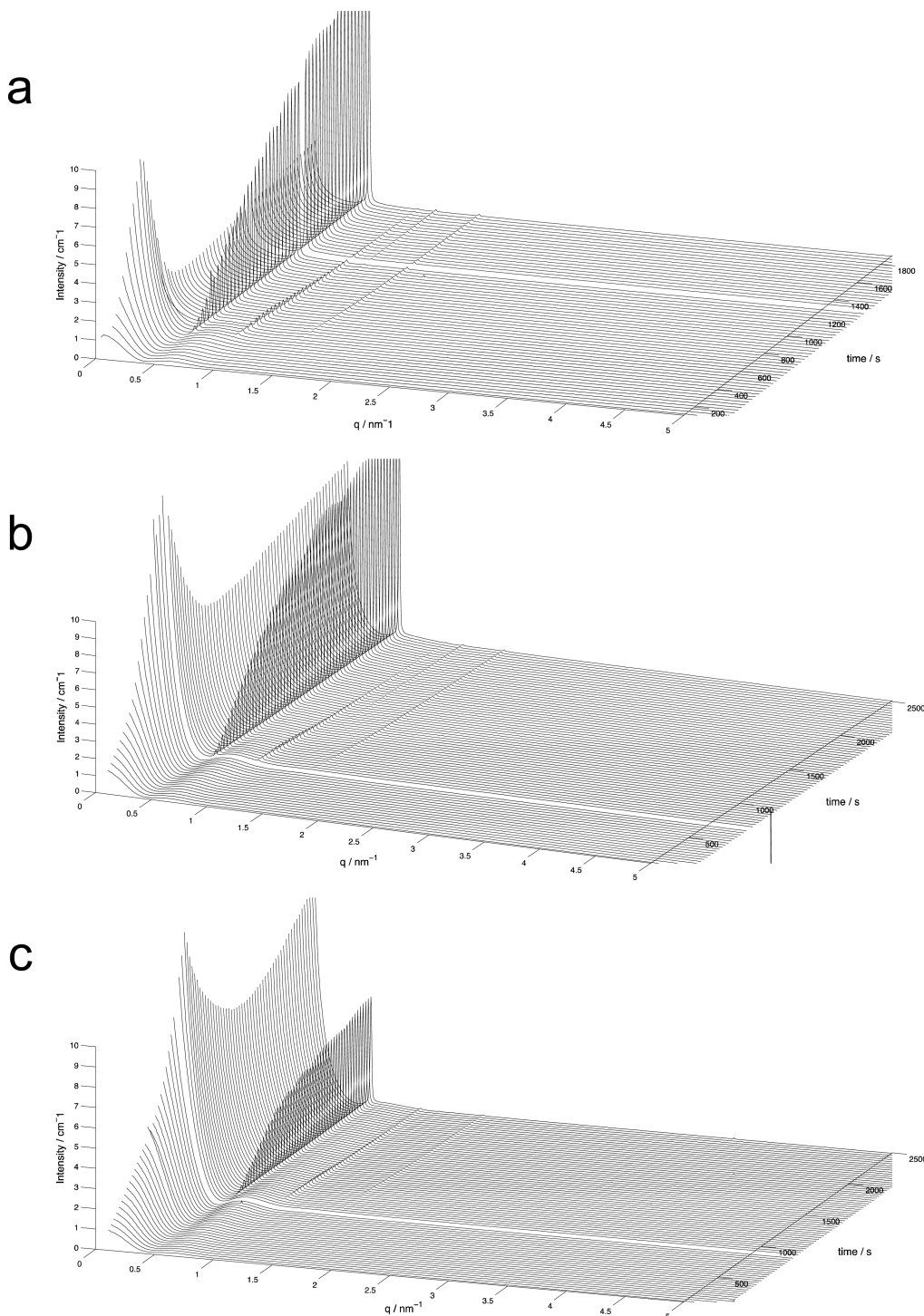


Figure 3. In-situ SAXS curves of the synthesis of (a) NaCl_0.5M, (b) SBA-15_ref, and (c) EtOH_0.5M. After an initial period with micellar scattering the hexagonal structure appears as evidenced by the emerging Bragg reflections. Although the formation events in the three cases are similar the timing of the events varies and it is clear that the time of appearance of the ordered phase varies depending on solvent conditions. The 10 peak appears after 7.5 min for NaCl_0.5M, 12 min for SBA-15_ref, and 17 min for EtOH_0.5M, respectively.

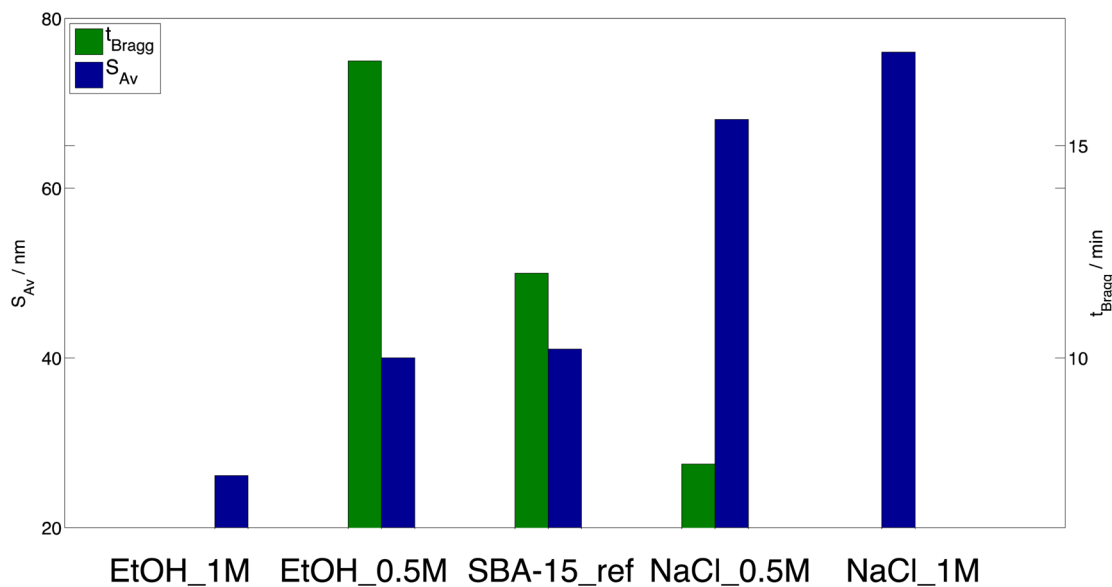
that the effect of tailing varies between the samples. The effect is clearly visible for samples EtOH_0.5M/1M, less so in the reference sample, while for NaCl_0.5M/1 M only a slight effect can be discerned. Hence, tailing gradually decreases as the polarity of the solvent increases.

We also note that the mesopores typically end by making a loop at the 001 face, a feature that was previously shown in another HRSEM study²¹ and also discussed by Linton et al.

considering the expected surface energies of particles synthesized at different temperatures.³⁵

The features resolved by the LV-HRSEM micrographs demonstrate that pore accessibility, also at the external 001 surface, is an issue that needs to be considered when applying SBA-15 for various applications. Although N₂-sorption can detect the presence of the plugs, their locations are only accessible from the LV-HRSEM data.

Scheme 1. Evolution of the Two Parameters t_{Bragg} and S_{Av} as the Solvent Conditions Are Changed by the Addition of EtOH or NaCl to the Synthesis Solution

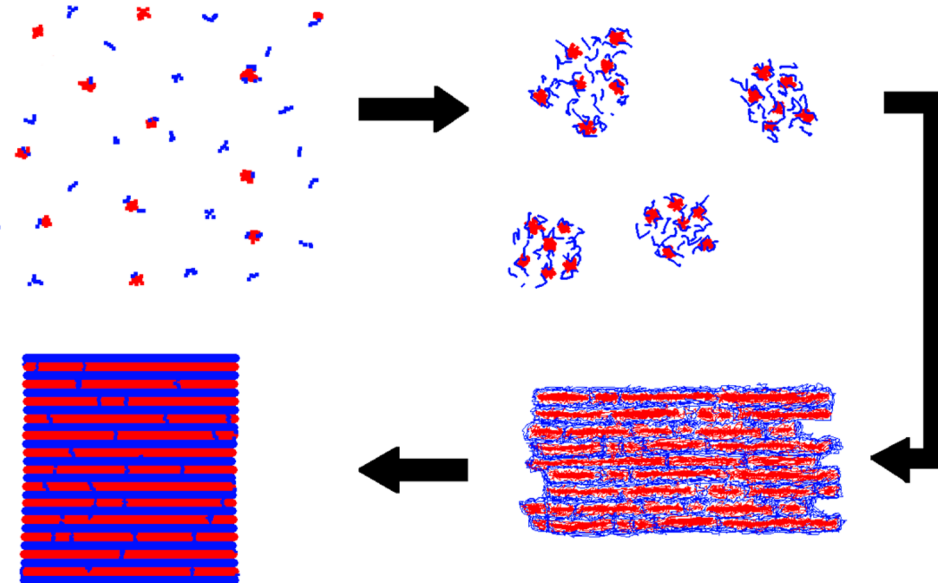


Study of Formation Dynamics. To relate the porosity characteristics to the formation dynamics, three syntheses, namely, those of SBA-15_ref, NaCl_0.5M, and EtOH_0.5M, were followed *in situ* through the use of X-rays at the SWING beamline at the SOLEIL synchrotron source. The results are presented in Figure 3. All three systems follow the same general sequence of formation events, as has previously been described.^{27,28} First an initial signal from the micelles in solution is observed. The intensity of this signal grows over time, as is expected when silica adheres to the corona,^{27,28} and eventually the signal shows the behavior at low q of cylindrical micelles. Bragg reflections, consistent with a 2D hexagonal structure ($p6mm$), appear as the material organizes into the ordered structure. The peaks continuously grow in intensity, meanwhile the micellar contribution to the scattering continuously decreases in intensity. The most obvious difference between the syntheses is the rate at which this sequence unfolds, most easily represented by the time of occurrence of the first Bragg reflection (the 10 peak). With 0.5 M NaCl present the Bragg reflection appears after 7.5 min, for the reference sample after 12 min, and with 0.5 M EtOH present it takes 17 min. Also, after 30 min of synthesis the micellar scattering is still visible for SBA-15_ref and even more so for EtOH_0.5M, whereas for the sample with NaCl it has disappeared. After the complete 24 h of synthesis this scattering is no longer discernible for any of the samples. SAXD spectra of samples that have undergone the complete synthesis procedure can be found in the Supporting Information, Figures S3–S7.

Formation of Plugs. We will now consider the combined results from these measurements relating the influence of solvent conditions to the formation of plugs within the pores of mesoporous SBA-15. Scheme 1 shows how the two parameters “Average distance between plugs”, S_{Av} , and “Time of appearance of Bragg reflection”, t_{Bragg} , vary depending on the solvent conditions. When the solubility of the Pluronic polymer decreases, that is, in the presence of NaCl, Bragg reflections appear quickly, indicating fast formation of the mesophase. For the same material after calcination, the average distance between plugs, as observed by LV-HRSEM analysis, increases.

In addition N_2 -sorption measurements indicate a relatively small tailing effect in the hysteresis. When ethanol is present, the situation is the reverse, that is, a delayed appearance of Bragg reflections, indicating slow formation of the mesophase, a decrease in the average distance between plugs, and a delayed desorption from the presence of plugs, that is, a pronounced tailing in the hysteresis.

The effect of different salts on the formation of SBA-15 have previously been studied with *in situ* SAXS.²⁸ The salt influenced the rate of formation of the mesophase, and the influence was in accordance with the Hoffmeister series. The intensity of the reflections increased in the presence of salting-out ions as compared to the salting-in ions. This was argued to be related to the fast formation rate. In a fast process the low degree of silica polymerization at the time of mesophase formation allows for a better arrangement and rearrangement of the micelles to form the hexagonal structure and hence a more well-defined structure. Contemporary work by Manet et al.,²⁷ including the use of an advanced fitting model to follow the evolution of the investigated process,³⁶ showed a more effective occlusion of siliceous network from the micellar corona in the presence of salting-out ions. These observations, combined with the results presented in this work, lead us to suggest the following to occur during the formation of SBA-15. After the fast hydrolysis of TMOS upon addition to the acidic micellar solution, the polymerizing siliceous species are attracted to the EO-corona of the Pluronic micelles. These silica-coated micelles will eventually form cylindrical micelles within the mesophase. Depending on the rate of mesophase formation, influenced by the presence of salt or ethanol, the silica will have a different degree of cross-linking at this time, thus being more or less flexible. Hence, the transformation from globular to long cylindrical micelles will not always be complete. One pore in the calcined material is not formed by a single cylindrical micelle. Rather it seems that several cylinders of different length are aligned in sequence, with each end-cap of the cylinders coated in silica. Therefore at each connection between sequential cylindrical segments there is a possibility for plug formation because of unsuccessful merging. In other words the

Scheme 2. Schematic Depiction of the Proposed Mechanism for the Formation of Plugs within the Pores of SBA-15^a

^aPluronic micelles are depicted in red, silica is depicted in blue, and the surrounding water as white. Initially small silica oligomers attach to the globular Pluronic micelles in solution, which is followed by an association of micelles within a loose siliceous network. The micelles elongate from globular to cylindrical but are not able to complete the transformation to single cylinders before the siliceous network becomes too rigid. Thus at the connections between sequential cylindrical micelles, remaining silica ends up forming plugs within the pores. Note the difference in density of the two bottom structures, which represents the decreasing water content as the formation process proceeds.

ongoing silica polymerization will arrest the structure before it reaches ideal cylinders, thus hindering micellar merging. This point in time is different under the different solvent conditions. The suggested mechanism is depicted in Scheme 2. The mechanism for plug formation that we propose differs from previous suggestions^{14–16} although a similar explanation was hinted on by Mandal and Kruk.³⁷ Note that the presence of additional species such as salt and alcohols is not the only way to influence solvent conditions. The typical method for forming plugged SBA-15 is by increasing the amount of the silica source used (typically TEOS). This directly increases the ethanol content and hence the solvent properties are changed. Another option would be to change the synthesis temperature, which influences the solubility of the Pluronic polymer. Note that a temperature change also influences the silica polymerization kinetics. This has been observed to affect the formation of plugs,¹⁸ and intrawall pores.³⁸ Since we propose that the plugs are formed as a natural consequence of the interaction between the polymerizing siliceous network and the EO-species of the Pluronic polymer, this mechanism can be used as a starting point to understand the presence of plugs no matter what experimental conditions are used.

Intrawall Pores in SBA-15. As was mentioned earlier, SBA-15 also contains a complementary set of pores, here referred to as intrawall pores, which connects the main mesopores, thus forming a 3D pore network. Figure 4 shows LV-HRSEM images of SBA-15_ref (synthesized with P104) and SBA-15_P123 (synthesized with P123) respectively. The images clearly show the presence of intrawall pores (examples indicated with white arrows) with a broad size distribution and, in addition, also the plugs and corrugations discussed above. SBA-15_P123 was used in a previous study where the amount of intrawall porosity was reduced without affecting the other properties of the material.³³ N₂-sorption data from that study also show some tailing at the closing of the hysteresis verifying

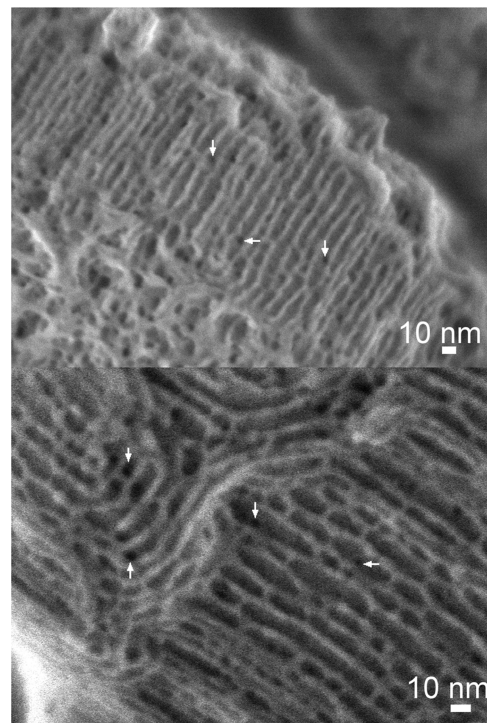


Figure 4. LV-HRSEM images of samples SBA-15_ref (top) and SBA-15_P123 (bottom). The white arrows indicate some of the pore openings of intrawall pores that exist in the pore walls of SBA-15. Both images were taken with a landing energy of 300 eV after applying a specimen bias of -5 kV. For the bottom image no Ar cleaning was applied before observation in the SEM.

the presence of plugs in SBA-15_P123 as well. Thus it is clear that the general features of SBA-15 are the same regardless of whether using P104 or P123 as structure director. It is then

reasonable to assume that these features will be more or less present in all SBA-15 materials synthesized using Pluronic polymers. To the best of our knowledge this is the first time the intrawall pores have been shown so clearly with a direct observation technique. The presence of intrawall pores is further supported by t-plots (Supporting Information, Figure S8–S9), which show significant amount of microporosity in both SBA-15_ref and SBA-15_P123. It should be mentioned that a comparative analysis such as a t-plot is dependent on the reference data used.³⁹ Such deviations that are observed at low pressures could possibly be eliminated through use of a better reference data.

CONCLUSION

In this work we have demonstrated how state of the art LV-HRSEM is a powerful tool in the analysis of porous materials. LV-HRSEM can, with great clarity, reveal several of the important material features, such as intrawall pores, pore corrugations, and plugs. We conclude that SBA-15 is a considerably more complex material than what is often described. In combination with N₂-sorption, the existence and frequency of occurrence of plugs in SBA-15 is analyzed. We demonstrate that the formation of the material, shown by *in situ* SAXS studies, is dependent on the solvent condition in the synthesis solution and that this is reflected in the porous properties.

ASSOCIATED CONTENT

Supporting Information

LV-HRSEM images, SAXD data, and t-plots (PDF). This material is available free of charge via the Internet at <http://pubs.acs.org>.

AUTHOR INFORMATION

Corresponding Author

*E-mail: tomas.kjellman@fkem1.lu.se.

Notes

The authors declare no competing financial interest.

ACKNOWLEDGMENTS

We gratefully acknowledged JEOL Ltd., Mr. Naoki Kikuchi and Mr. Yusuke Sakuda for assistance with the LV-HRSEM operation and Dr. Alfonso Garcia-Bennett, Stockholm University, for his assistance with the pore size determination. Financial support by the Swedish Foundation for Strategic Research (T.K. and V.A.), the Swedish Research Council through the Linnaeus grant “Organizing Molecular Matter” (V.A. and T.K.), Kungliga Fysiografiska Sällskapet for a travel grant (T.K.), and an individual project grant from the Swedish Research Council (V.A.).

REFERENCES

- (1) Zhao, D.; Huo, Q.; Feng, J.; Chmelka, B. F.; Stucky, G. D. *J. Am. Chem. Soc.* **1998**, *120* (24), 6024–6036.
- (2) Beck, J. S.; Vartuli, J. C.; Roth, W. J.; Leonowicz, M. E.; Kresge, C. T.; Schmitt, K. D.; Chu, C. T. W.; Olson, D. H.; Sheppard, E. W. *J. Am. Chem. Soc.* **1992**, *114* (27), 10834–10843.
- (3) Inagaki, S.; Fukushima, Y.; Kuroda, K. *J. Chem. Soc., Chem. Commun.* **1993**, *8*, 680–682.
- (4) Rosenholm, J. M.; Sahlgren, C.; Lindén, M. *Nanoscale* **2010**, *2* (10), 1870–1883.
- (5) Kumar, P.; Guliants, V. V. *Microporous Mesoporous Mater.* **2010**, *132* (1–2), 1–14.
- (6) Taguchi, A.; Schüth, F. *Microporous Mesoporous Mater.* **2005**, *77* (1), 1–45.
- (7) Vasiliev, P. O.; Shen, Z.; Hodgkins, R. P.; Bergström, L. *Chem. Mater.* **2006**, *18* (20), 4933–4938.
- (8) Melosh, N. A.; Lipic, P.; Bates, F. S.; Wudl, F.; Stucky, G. D.; Fredrickson, G. H.; Chmelka, B. F. *Macromolecules* **1999**, *32* (13), 4332–4342.
- (9) Ryoo, R.; Ko, C. H.; Kruk, M.; Antochshuk, V.; Jaroniec, M. *J. Phys. Chem. B* **2000**, *104* (48), 11465–11471.
- (10) Kruk, M.; Jaroniec, M.; Ko, C. H.; Ryoo, R. *Chem. Mater.* **2000**, *12* (7), 1961–1968.
- (11) Jun, S.; Joo, S. H.; Ryoo, R.; Kruk, M.; Jaroniec, M.; Liu, Z.; Ohsuma, T.; Terasaki, O. *J. Am. Chem. Soc.* **2000**, *122* (43), 10712–10713.
- (12) Fan, J.; Yu, C.; Wang, L.; Tu, B.; Zhao, D.; Sakamoto, Y.; Terasaki, O. *J. Am. Chem. Soc.* **2001**, *123* (48), 12113–12114.
- (13) Galarneau, A.; Cambon, H.; Di Renzo, F.; Ryoo, R.; Choi, M.; Fajula, F. *New J. Chem.* **2003**, *27* (1), 73–79.
- (14) Van Der Voort, P.; Ravikovitch, P. I.; De Jong, K. P.; Neimark, A. V.; Janssen, A. H.; Benjelloun, M.; Van Bavel, E.; Cool, P.; Weckhuysen, B. M.; Vansant, E. F. *Chem. Commun.* **2002**, *9*, 1010–1011.
- (15) Van Der Voort, P.; Ravikovitch, P. I.; De Jong, K. P.; Benjelloun, M.; Van Bavel, E.; Janssen, A. H.; Neimark, A. V.; Weckhuysen, B. M.; Vansant, E. F. *J. Phys. Chem. B* **2002**, *106* (23), 5873–5877.
- (16) Kruk, M.; Jaroniec, M.; Joo, S. H.; Ryoo, R. *J. Phys. Chem. B* **2003**, *107* (10), 2205–2213.
- (17) Reichhardt, N. V.; Guillet-Nicolas, R.; Thommes, M.; Klosgen, B.; Nylander, T.; Kleitz, F.; Alfredsson, V. *Phys. Chem. Chem. Phys.* **2012**, *14* (16), 5651–5661.
- (18) Celer, E. B.; Kruk, M.; Zuzek, Y.; Jaroniec, M. *J. Mater. Chem.* **2006**, *16* (27), 2824–2833.
- (19) Tüysüz, H.; Lehmann, C. W.; Bongard, H.; Tesche, B.; Schmidt, R.; Schüth, F. *J. Am. Chem. Soc.* **2008**, *130* (34), 11510–11517.
- (20) Stevens, S. M.; Jansson, K.; Xiao, C.; Asahina, S.; Klingstedt, M.; Grüner, D.; Sakamoto, Y.; Miyasaka, K.; Cubillas, P.; Brent, R.; Han, L.; Che, S.; Ryoo, R.; Zhao, D.; Anderson, M.; Schüth, F.; Terasaki, O. *JEOL News* **2009**, *44* (1), 17–22.
- (21) Che, S.; Lund, K.; Tatsumi, T.; Iijima, S.; Joo, S. H.; Ryoo, R.; Terasaki, O. *Angew. Chem., Int. Ed.* **2003**, *42* (19), 2182–2185.
- (22) Howard, G. J.; McConnell, P. *J. Phys. Chem.* **1967**, *71* (9), 2974–2981.
- (23) Grant, L. M.; Tiberg, F.; Ducker, W. A. *J. Phys. Chem. B* **1998**, *102* (22), 4288–4294.
- (24) Malmsten, M.; Linse, P.; Cosgrove, T. *Macromolecules* **1992**, *25* (9), 2474–2481.
- (25) Flodstrom, K.; Wennerstrom, H.; Alfredsson, V. *Langmuir* **2004**, *20* (3), 680–688.
- (26) Zhang, W.-H.; Zhang, L.; Xiu, J.; Shen, Z.; Li, Y.; Ying, P.; Li, C. *Microporous Mesoporous Mater.* **2006**, *89* (1–3), 179–185.
- (27) Manet, S.; Schmitt, J.; Impérator-Clerc, M.; Zholobenko, V.; Durand, D.; Oliveira, C. L. P.; Pedersen, J. S.; Gervais, C.; Baccile, N.; Babonneau, F.; Grillo, I.; Meneau, F.; Rochas, C. *J. Phys. Chem. B* **2011**, *115* (39), 11330–11344.
- (28) Teixeira, C. V.; Amenitsch, H.; Linton, P.; Lindén, M.; Alfredsson, V. *Langmuir* **2011**, *27* (11), 7121–7131.
- (29) Alexandridis, P.; Alan Hatton, T. *Colloids Surf. A* **1995**, *96* (1–2), 1–46.
- (30) Alexandridis, P.; Holzwarth, J. F. *Langmuir* **1997**, *13* (23), 6074–6082.
- (31) Parekh, P.; Singh, K.; Marangoni, D. G.; Bahadur, P. *J. Mol. Liq.* **2012**, *165* (0), 49–54.
- (32) Kabalnov, A.; Olsson, U.; Wennerström, H. *J. Phys. Chem.* **1995**, *99* (16), 6220–6230.
- (33) Kjellman, T.; Reichhardt, N.; Sakeye, M.; Smått, J.-H.; Lindén, M.; Alfredsson, V. *Chem. Mater.* **2013**, *25* (9), 1989–1997.
- (34) Thommes, M. *Chem. Ing. Tech.* **2010**, *82* (7), 1059–1073.

- (35) Linton, P.; Hernandez-Garrido, J.-C.; Midgley, P. A.; Wenniferstrom, H.; Alfredsson, V. *Phys. Chem. Chem. Phys.* **2009**, *11* (46), 10973–10982.
- (36) Sundblom, A.; Oliveira, C. L. P.; Palmqvist, A. E. C.; Pedersen, J. S. *J. Phys. Chem. C* **2009**, *113* (18), 7706–7713.
- (37) Mandal, M.; Kruk, M. *Chem. Mater.* **2011**, *24* (1), 149–154.
- (38) Celer, E. B.; Jaroniec, M. *J. Am. Chem. Soc.* **2006**, *128* (44), 14408–14414.
- (39) Jaroniec, M.; Kruk, M.; Olivier, J. P. *Langmuir* **1999**, *15* (16), 5410–5413.